Biochimica et Biophysica Acta 1817 (2012) 1471–1482

Contents lists available at SciVerse ScienceDirect

Biochimica et Biophysica Acta

journal homepage: www.elsevier.com/locate/bbabio

A comparative spectroscopic and kinetic study of photoexcitations in detergent-isolated and membrane-embedded LH2 light-harvesting complexes ☆

Arvi Freiberg [a,b,c,*], Margus Rätsep [a], Kõu Timpmann [a]

[a] Institute of Physics, University of Tartu, Riia 142, Tartu 51014, Estonia
[b] Institute of Molecular and Cell Biology, University of Tartu, Riia 23, Tartu 51010, Estonia
[c] Estonian Academy of Sciences, Kohtu 6, Tallinn 10130, Estonia

ARTICLE INFO

Article history:
Received 4 October 2011
Received in revised form 18 November 2011
Accepted 22 November 2011
Available online 8 December 2011

Keywords:
Bacterial photosynthesis
Light-harvesting antenna
Exciton
Membrane-bound LH2
Exciton–phonon coupling
Energy transfer

ABSTRACT

Integral membrane proteins constitute more than third of the total number of proteins present in organisms. Solubilization with mild detergents is a common technique to study the structure, dynamics, and catalytic activity of these proteins in purified form. However beneficial the use of detergents may be for protein extraction, the membrane proteins are often denatured by detergent solubilization as a result of native lipid membrane interactions having been modified. Versatile investigations of the properties of membrane-embedded and detergent-isolated proteins are, therefore, required to evaluate the consequences of the solubilization procedure. Herein, the spectroscopic and kinetic fingerprints have been established that distinguish excitons in individual detergent-solubilized LH2 light-harvesting pigment–protein complexes from them in the membrane-embedded complexes of purple photosynthetic bacteria *Rhodobacter sphaeroides*. A wide arsenal of spectroscopic techniques in visible optical range that include conventional broadband absorption–fluorescence, fluorescence anisotropy excitation, spectrally selective hole burning and fluorescence line-narrowing, and transient absorption–fluorescence have been applied over broad temperature range between physiological and liquid He temperatures. Significant changes in energetics and dynamics of the antenna excitons upon self-assembly of the proteins into intracytoplasmic membranes are observed, analyzed, and discussed. This article is part of a Special Issue entitled: Photosynthesis Research for Sustainability: from Natural to Artificial.

1. Introduction

Integral membrane proteins are ubiquitous in many life-supporting functions, such as selective transmission of information and matter across the membrane, immune response, photosynthesis, and respiration. Solubilization with mild detergents is a common technique to study the structure, dynamics, and catalytic activity of these proteins in purified form. However beneficial the use of detergents may be for protein extraction, the membrane proteins are often inactivated by detergent solubilization as a result of native lipid membrane interactions having been modified. Versatile comparative investigations of the properties of native membrane-embedded and detergent-isolated membrane proteins are, therefore, required to evaluate the consequences of the procedure [1].

The biological machinery driving photosynthesis comprises an elaborate assemblage of membrane proteins that include chlorophylls and carotenoids as the main harvesters of sunlight [2]. The purple non-sulfur bacterium *Rhodobacter (Rb.) sphaeroides* is one of the best-characterized photosynthetic species due to its genetic and physiological flexibility [3,4]. The light harvesting (LH) antenna pigment–protein complexes of the photosynthetic bacteria are among the most studied membrane proteins; they absorb solar photons and transfer the resulting exciton energy to the photochemical reaction center (RC), where it is transformed into potential chemical energy [5]. The relative spatial arrangement of the antenna and RC complexes has been determined by spectroscopic methods [6,7] and notably by atomic force microscopy [8–12]. In the wild type purple non-sulfur bacterium *Rb. sphaeroides*, the photosynthetic apparatus is organized into intracytoplasmic chromatophore vesicles of nearly spherical shape of 50–60 nm diameter [13]. The core LH1 and

Abbreviations: LH, light harvesting complex; RC, reaction center; Bchl, bacteriochlorophyll; *Rb.*, *Rhodobacter*; *Rps.*, *Rhodopseudomonas*; Tris, tris-hydrixymethyl-aminomethane; EDTA, ethylene–diamine–tetraacetic acid; LDAO, dodecyl–dimetyl–amine oxid; Q_y, lowest singlet electronic transition; OD, optical density; HB, hole burning; FLN, fluorescence line narrowing; ΔFLN, differential fluorescence line narrowing; DLS, dynamic light scattering; FWHM, full width at half maximum; ZPL, zero-phonon line; SDF, state distribution function; PW, phonon wing; S, exciton–phonon coupling strength; Q, fluorescence yield; τ, fluorescence decay time; DOS, distribution of the exciton states; ESA, excited-state absorption; GSA, ground state absorption; SE, stimulated emission

☆ This article is part of a Special Issue entitled: Photosynthesis Research for Sustainability: from Natural to Artificial.

* Corresponding author. Institute of Physics, University of Tartu, 51014 Tartu, Estonia. Tel.: +372 56453175; fax +372 7 383 033.
E-mail address: arvi.freiberg@ut.ee (A. Freiberg).

0005-2728/$ – see front matter © 2011 Elsevier B.V. All rights reserved.
doi:10.1016/j.bbabio.2011.11.019

peripheral LH2 light-harvesting complexes, along with a smaller number of the RC complexes, mainly populate the chromatophore membranes. The success of photosynthesis thus depends on ultrafast events, in which up to hundreds of membrane proteins are cooperating in a multistep process of solar energy funneling to the RC. The basic building block of the peripheral LH2 antenna protein complex from *Rhodopseudomonas (Rps.) acidophila* is a heterodimer of α-helical α- and β-apoproteins, each non-covalently binding three bacteriochlorophyll *a* (Bchl) molecules [14]. Build-up of the LH2 complexes from *Rb. sphaeroides* is similar [15,16]. A remarkable feature of the organization of the 27 Bchl molecules in the 9-membered LH2 rings is their partition into two concentric pools. Eighteen of the Bchl molecules form a ring of overlapping Bchls in a water-wheel arrangement. The other 9 pigments in the opposite side of the membrane are more loosely packed. These molecules also have their bacteriochlorin planes oriented perpendicular to the symmetry axis of the protein.

In the present work, optical spectral and ultrafast (subpicosecond to nanosecond) kinetic responses that accompany self-assembly of the peripheral LH2 antenna complexes from *Rb. sphaeroides* into extended, genetically modified membrane vesicles containing associations of LH2 as the sole LH complexes (further dubbed as membranes) in buffer solution are systematically studied. When corresponding data are available, useful comparison with the LH2 and LH3 complexes from *Rps. acidophila* are made. The different spectroscopic techniques applied to distinguish spectrally and kinetically the individual purified LH2 complexes from their interconnected membrane-embedded ensembles include conventional broadband absorption–fluorescence emission, fluorescence anisotropy excitation, spectrally selective hole burning and fluorescence line-narrowing, and transient absorption and fluorescence. The studies have been carried out in a wide temperature range spanning from liquid He to physiological temperatures. Low temperatures and spectrally selective methods are necessary for uncovering homogenous spectral characteristics from inhomogeneously broadened ensemble spectra.

Spectroscopic properties of the LH2 complexes in buffer–detergent solution have been extensively studied (see, e.g., [5,17–34] for representative examples). While free in organic solvents, the lowest singlet (Q_y) electronic transition of the Bchl molecule is located in the near-infrared region at ~775 nm [35]. Significant red shifts (moves toward lower energy) of this transition are observed in the antenna systems: the 9 loosely packed Bchl molecules give rise to an absorption at 800 nm (the B800 band), while the 18 tightly packed pigments, to an absorption at 850 nm (the B850 band). The prime origin of these red shifts is interactions between the transition densities of the Bchl molecules along with the interactions between each Bchl and the surrounding protein. The former couplings cause the so-called exciton shift due to stabilization of the delocalized excited state, while the latter interactions lead to the solvent/protein shift. Universal dispersion couplings aside, the factors that contribute most into the protein shift are hydrogen bonding and various conformational interactions. The position of the Bchl Q_y transition thus constitutes a sensitive intrinsic molecular probe that is able to monitor both the state of intermolecular couplings and the supramolecular organization of the antenna protein complexes with sub-nanometer spatial resolution [36]. Although extra red shifts of the absorption spectra, related to self-assembly of the antenna pigment–protein complexes into photosynthetic membrane are routinely observed, comparative studies of the spectral properties of the individual LH2 complexes and their membrane-embedded ensembles have been relatively rare as well as fragmented [22,31,37–43].

2. Experimental

2.1. Samples

The purified into detergent micelles and self-assembled into native photosynthetic membrane vesicles LH2 complexes from *Rb. sphaeroides* 2.4.1 strain were prepared as described earlier [44–46]. Cultures of a *Rb. sphaeroides* strain with deleted antenna and reaction center genes were grown semiaerobically in a rich medium. After harvesting, the cells were resuspended in TEN (20 mM Tris–HCl buffer at pH 8.0 containing 1 mM EDTA and 0.1 M NaCl) and lysed at 20,000 psi in a French pressure cell. The cell extracts were incubated with DNAse and then centrifuged for 30 min at 8000 rpm (Sorvall GS3 rotor) to remove whole cells and debris. The LH2 complexes were isolated by high-speed 45,000 rpm centrifugation for 16 h (Beckman Ti45 rotor) on a 0.3, 0.6 and 1.2 M sucrose step gradient containing TEN and 0.2% LDAO. The final preparations were suspended in a TEN to yield a desired absorbance in the experimental cell. The samples for low-temperature/temperature-dependent studies were prepared by dilution with glycerol (1:2 volume ratio). In this case also the detergent (LDAO) concentration was increased to ~1% to maintain the LH2 complexes as well separated units over long period of experimental time [1,47]. As shown in [31], adding glycerol slightly stabilizes (red-shifts) the room-temperature spectra of preparations from *Rb. sphaeroides*, but practically does not influence the spectra of those from *Rps. acidophila*.

2.2. Steady-state spectroscopy

The absorption spectra of LH2 complexes and membranes were taken using spectrophotometer Jasco V-570 (Jasco Corporation).

The emission spectra measurements were performed with the system consisting of Ti:sapphire solid state laser (model 3900S, Spectra Physics) pumped by an Ar^+ ion laser (model 171, Spectra Physics) and a 0.3 m spectrograph (Shamrock SR-303i, Andor Technology) equipped with an electrically cooled CCD camera (DV420A-OE, Andor Technology). The spectral resolution of measurements varied between 0.1 and 0.8 nm, depending on the grating applied. The wavelength scale of the spectrometer was determined with the precision of ± 0.1 nm by a calibration lamp. The emission spectra were recorded at 90° geometry with respect to the excitation light beam. The spectra were corrected for the spectral sensitivity of the detection system. Measurements at low temperatures were performed in a liquid helium cryostat (Utreks) equipped with a temperature control system. The sample solution, fixed between two quarts plates about 1.5 mm apart or in 4 mm diameter gelatin capsules, was slowly cooled down to 5 ± 0.5 K. The temperature dependences were generally measured from higher to lower temperatures to avoid confusion due to characteristic hysteresis of spectral parameters, typical for glassy systems. Care was taken to avoid reabsorption effects on the fluorescence emission spectra (as well as on fluorescence decay times) due to high optical density (OD) of the specimen. OD of the samples used for these measurements was generally below 0.1 (recorded at B850 absorption band maximum at ambient temperature).

For anisotropy measurements the emitted light path was equipped with two polarizers. The first one was used as an analyzing polarizer, which direction was turned to either parallel or perpendicular with respect of vertically polarized excitation beam. The second one, installed at 45° to polarization of excitation beam was used to correct the polarization data due to the influence of the detection system. The fluorescence anisotropy spectrum was calculated according to the following equation:

$$r(\omega) = \frac{I_{vv}(\omega) - I_{vh}(\omega)}{I_{vv}(\omega) + 2I_{vh}(\omega)}, \quad (1)$$

where $I_{vv}(\omega)$ and $I_{vh}(\omega)$ are the fluorescence intensities polarized, respectively, in parallel (index *vv*) and perpendicular (*vh*) with respect to the vertically linearly polarized excitation light.

In high-resolution hole burning (HB) [48], fluorescence line narrowing (FLN) [48], and differential FLN (ΔFLN) [49] measurements

the excitation laser linewidth was 0.5 cm^{-1}. For HB transmission measurements, a high stability tungsten lamp source BPS100 (BWTek) was used. The burning laser intensity and burning times were adjusted, respectively, between 0.2 and 100 mW/cm^2 and between 10 and 300 s to find proper holes without saturating the sample. No degradation of the samples or nonlinear excitation effects was observed at average excitation light intensities ≤100 mW/cm^2.

2.3. Transient femto-picosecond spectroscopy

The applied femtosecond differential absorption spectrometer setup has been described [46]. Briefly, a commercially available 1 kHz repetition rate Ti: Sapphire Regenerative Amplifier (Model CPA-1000, Clark-MXR) was used as a source of femtosecond light pulses at 775 nm. The split source pulses were utilized to generate tunable pump pulses in an optical parametric amplifier (OPA) (Clark-MXR) and to produce spectral continuum for the probe and reference pulses. The 12–15 nm wide OPA pulses were further narrowed to 4–5 nm by using band-pass interference filters (Omega Optical) resulting in ~200 fs spectral bandwidth-limited pump pulses. The angle between linearly polarized pump and probe beams was 54.7°. A stepping motor-driven delay line controlled the variable time delay between the probe/reference and pump pulses. The spectral content of the sample response was recorded with 1 nm resolution using the SpectraPro-275 spectrograph (Acton Research) equipped with a dual array CCD detector (ST-121, Princeton Instruments).

The picosecond emission spectrometer (picosecond spectrochronograph) used has been described [50,51]. In the present version, it consists of a Coherent 700 styryl-9M mode-locked dye laser, synchronously pumped at 76 MHz by a Coherent Antares 76S Nd-YAG laser as an excitation source with 3–5 ps pulsewidth, a subtractive-dispersion double-grating monochromator (LOMO), as a spectral analyzer, and a home-built synchroscan streak camera as a fast detector. The streak camera was linked via a vidicon to an OSA 500 Optical Spectrum Analyzer (B&M Spektronik). The scattering from the sample at excitation wavelength was recorded and used as an instrument response function. Low pulsed excitation light intensity was applied to avoid excited-state lifetime distortions due to singlet-singlet or singlet triplet annihilation [52,53].

Global as well as simple one-wavelength analysis of the kinetics has been performed. The decay times, τ, were calculated using a least squares fitting algorithm assuming multi-exponential kinetics and taking into account the finite instrument response function (200 fs for femtosecond measurements and 20–25 ps for picosecond measurements). The time resolved fluorescence emission spectra, $I(\lambda,t)$, were built as

$$I(\lambda,t) = \sum_i A_i(\lambda)\exp\left[-\frac{t}{\tau_i(\lambda)}\right], \quad (2)$$

where the sum was taken over the number of kinetic components used in the fitting procedure (see [54] for more details).

3. Results and discussion

3.1. Sample characterization by dynamic light scattering

Dynamic light scattering (DLS) [55] was used to characterize aggregation state and size of the LH2 complexes in the sample solution at ambient temperature (25 °C). In this technique, a laser light scattered by a diffusing particle is analyzed in terms of the temporal field autocorrelation function. From the known dependence of the correlation function measured over a wide range of times on the diffusion properties of the particles, a distribution of hydrodynamic radii, R_h, of the scattering units can be obtained.

The results obtained by applying a DynaPro-MS/X (Protein-Solutions Inc.) particle-sizing instrument are shown in Fig. 1. The data meet ones expectations that hydrodynamic radii of the vesicular membrane particles and detergent-isolated LH2 complexes are very different. The histogram for the membrane vesicles (Fig. 1a) contains a single band centered at $R_h = 64 \pm 16$ nm. Significantly smaller radius of 26.5 nm has been found in [16] applying the statistically probably less reliable atomic force microscopy technique. The solution of isolated LH2 complexes (Fig. 1b) reveals three bands corresponding to $R_h = 3.0 \pm 0.5$ nm, $R_h = 72 \pm 22$, and $R_h = 2910$ nm. It is known that the larger particles scatter light much stronger than do the smaller particles, therefore, greatly exaggerating their prominence in the scattering spectrum. Therefore, relative masses of the particles are also indicated by red histograms in Fig. 1b (scale in the right hand side). As seen, the left-most peak at $R_h = 3.0 \pm 0.5$ nm by far dominates (>99%) the spectrum in terms of the overall mass of scattering particles. Judging by rough agreement with the size of the detergent-stabilized LH2 complexes of *Rb. sphaeroides* estimated from the small angle X-ray scattering data [56], it can be assigned to isolated LH2 complexes. This radius is also consistent with the 6.2 nm diameter of the complexes reconstructed from electron micrographs of the two-dimensional crystals [15]. The rest two bands at $R_h = 72 \pm 22$ nm and $R_h = 2910$ nm, being minor by mass (<<1%), correspond to the membrane traces and the occasional dust, respectively. We thus conclude that the solution in Fig. 1b primarily contains well-isolated LH2 antenna complexes.

3.2. Conventional steady-state absorption and fluorescence emission spectra

Fig. 2 demonstrates conventional (low-resolution) steady-state absorption and non-selectively excited fluorescence emission spectra of isolated and membrane LH2 complexes measured at ambient

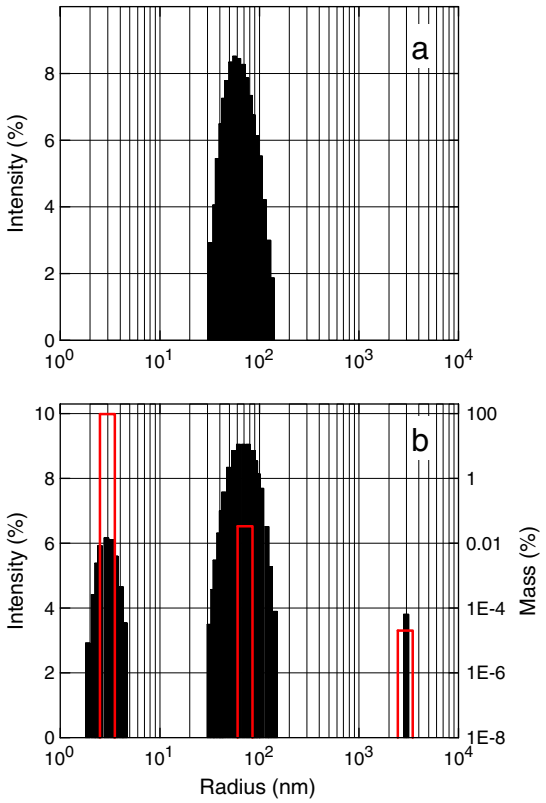

Fig. 1. Distributions of hydrodynamic radii of the particles found in solutions of LH2-binding membrane vesicles (a) and detergent micelles (b) at ambient temperature. Red histograms present relative masses of the particles (right scale).

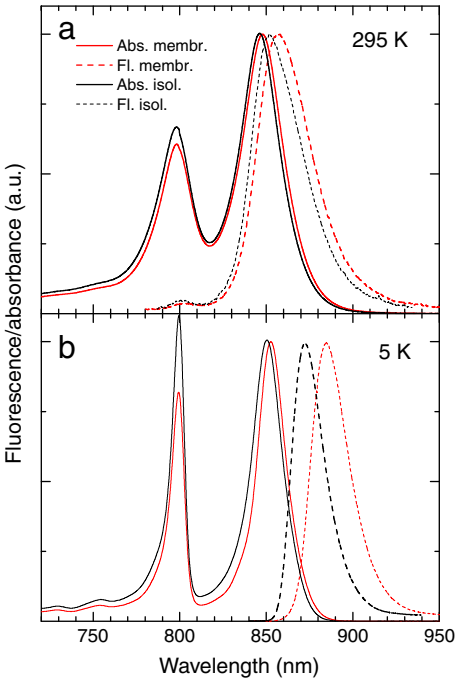

Fig. 2. The Q_y absorption (continuous line) and fluorescence emission (dashed line) spectra of a solution of isolated (black line) and membrane (red line) LH2 complexes recorded at ambient temperature (a) and at 5 K (b). The fluorescence spectra are non-selective excited into the Q_x absorption maximum at 590 nm. All the spectra have been normalized with respect to the B850 absorption/fluorescence band maximum.

temperature (Fig. 2a) and at 5 K (Fig. 2b). Visible in the absorption spectra are two main bands: the B800 band with a peak at about 800 nm and the B850 band that absorbs around 850 nm. As already explained in Introduction, both these bands are related to the Q_y electronic transition in individual Bchl molecules. The notable spectral variance of the two bands is due to separate Bchl associations in the LH2 structure that support different type of excitations. Responsible for the B800 band are 9 Bchl molecules in loose arrangement, whereas the 18 strongly excitonically coupled Bchl molecules give raise the B850 band [5,20,21,23]. In membranes the B850 band is a few nanometers (1.1 nm at 295 K and 3.3 nm at 5 K) more red shifted than in isolated complexes. The B800 absorption band of mostly localized excitations seems not to feel this subtle change of the surroundings. The B850 band is generally also wider than the B800 band. Selective and single-molecule spectroscopy data agree in showing that while the latter band is inhomogeneously broadened, the former band is largely homogeneous [21,29]. The long-wavelength limit of the exciton absorption band at around 890–900 nm is clearly seen in the 5 K spectra. At ambient temperatures the red tail of the spectrum is more extended, one reason being the anti-Stokes absorbance from the thermally populated ground-state vibrational levels (see below).

The Stokes-shifted fluorescence emission is related to the B850 absorption band, being thus basically of the exciton polaron/self-trapped exciton origin [23,57,58]. Only at close to ambient temperatures a weak additional shoulder around 802 nm can be noticed. This feature is due to thermally populated B800 states and it rapidly fades out with decreasing temperature, becoming immeasurable weak at 5 K [52,59]. The Stokes shift between the absorption and fluorescence spectra changes with temperature: it is generally much larger in membranes than in isolated complexes due to connectivity between the membrane light-harvesting complexes (see below). Except lowest temperatures, the fluorescence spectra are wider compared with the respective absorption spectra. Since mostly the B850 states are active in physiological energy transfer pathways [23], we shall further primarily concentrate on this (exciton) sub-system.

Fig. 3 reveals strikingly different temperature dependences of the B850 absorption and fluorescence emission spectra. The spectra are characterized by just two parameters, their peak energy and bandwidth; the latter being defined as full width at half maximum, FWHM. While there is only a few nanometers red shift and some narrowing of the absorption spectra upon decreasing temperature both in isolated and membrane samples, the changes in fluorescence emission spectra are relatively huge. Similar spectral disparities in the case of isolated LH2 complexes from *Rps. acidophila* have recently been

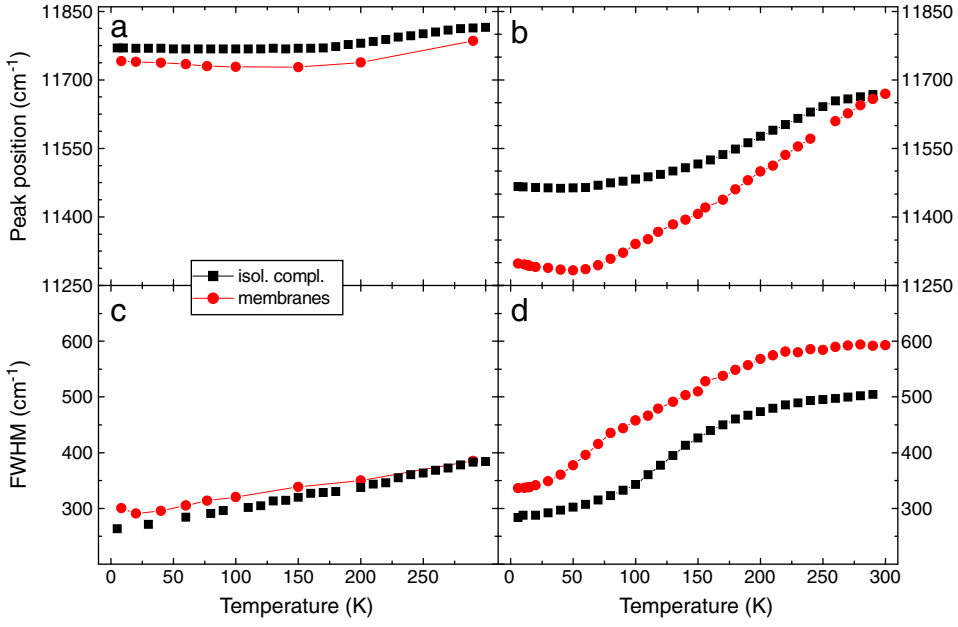

Fig. 3. Temperature dependence of peak positions (a, b) and bandwidths (c, d) of the low-resolution B850 absorption (a, c) and fluorescence emission (b, d) spectra for isolated (black symbols) and membrane-embedded (red symbols) LH2 complexes. The fluorescence is excited at 590 nm. The solid lines connecting the scattered data points are for leading the eye.

successfully explained [58] taking into account distinct origin of the photo-excitations that give raise to absorption and fluorescence emission spectra.

Comparing separately the absorption and fluorescence spectral dependences for isolated and membrane complexes, the differences are subtle, but still notable. The spectra of membrane particles are systematically redder (i) as well as broader (ii), their fluorescence spectra showing much more prominent temperature dependence both in terms of the positional shift rate (iii) as well as deepness of the red-shift irregularity at intermediate temperatures (10–70 K) (iv). It is important to notice that these differences are insensitive to the direction of the temperature change, from higher to lower or vice versa.

As we will show shortly (see Fig. 4), the features (i) and (ii) equally speak for somewhat loosened protein structure, consequently, a smaller exciton coupling energy in detergent micelles compared with that in intact membrane surroundings. This conclusion correlates also well with the fact that the membrane LH2 complexes from *Rb. sphaeroides* are more resistant than the isolated complexes against externally applied high pressure [22,41].

Estimates of the exciton coupling energy in cyclic bacterial antennas can be obtained from the fluorescence anisotropy excitation spectra [60,61]. Fig. 4 shows the result of such measurements for isolated and membrane LH2 complexes, where the two anisotropy dips, one at low, another at high energy, mark the edges of the exciton state manifolds [58]. While the high-energy dips at 763.0 nm in the two samples practically coincide, the low-energy dips (at 843.5 nm in isolated complexes and at 846.8 nm in membrane complexes) are shifted relative to each other by 3.3 nm, which is precisely the relative sift between respective absorption bands. The same mechanism (shrinkage of the exciton band, from 1297 cm^{-1} in membranes to 1251 cm^{-1} in isolated complexes) also explains narrower B850 absorption band in isolated complexes. It is of notice that in contrast to *Rb. sphaeroides*, the isolated and native membrane-embedded LH2 complexes from *Rps. acidophila* have almost identical absorption spectra and, consequently, exciton bandwidth (unpublished data).

The features (iii) and (iv) requires more involved discussion. As can be seen from Figs. 2 and 3b, the B850 fluorescence band positions for isolated and membrane samples have rather different temperature dependence. While the band peaks almost coincide at ambient temperature, they are at 5 K separated by 169 cm^{-1}. Advanced red shift of the fluorescence peak in membranes (feature (iii)) is expected due to the ability of energy transport along the inter-connected network of the LH2 complexes, and resulting excitation energy concentration into the lowest-energy ensemble states [45,46,52,62–65]. Somewhat surprising, however, is that such energy funneling does not lead to simultaneous narrowing of the membrane emission spectra relative to the spectra of isolated complexes (see Fig. 3d). The most probable reason for this is the well-known structural heterogeneity of the membranes restraining the excitation energy transfer. Instead of reaching the lowest-energy states, the excitons at low temperatures may have stuck in local minima of the rough potential energy surface corresponding to specific LH2 associations/conformations. Existence of multiple antenna protein rafts has been documented by atomic force microscopy [8–11,16,66,67]. Occurrence of a minimum around 50 K in the temperature dependence of the fluorescence band position (feature (iv)) implies presence of at least two competing with each other band-shift mechanisms. As shown in [58], the dominant factor determining the fluorescence band shape at higher temperatures is thermal population of the upper-energy exciton polaron states. In contrast, the blue shifting of the fluorescence peaks below ~50 K is related to the emergence at low temperatures of intense zero-phonon lines (ZPL) at origins of the homogenous spectra [68]. The prominence of the blue shift in membrane spectra is explained by their larger inhomogeneous width (see Fig. 3d). We shall elaborate these subtleties in more detail in subsequent Sections 3.3 and 3.4.

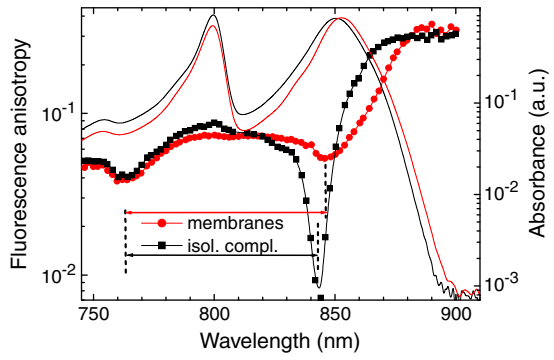

Fig. 4. Fluorescence anisotropy excitation spectra of detergent-isolated (black squares) and membrane-embedded (red dots) LH2 complexes at 4.5 K. The vertical dashed lines connected with black and red arrows indicate the positions of the anisotropy dips. The absorption spectra of the same samples drawn with black and red lines, respectively, are shown for reference. Note logarithmic vertical scales used for amplification the low-intensity parts of the spectra.

3.3. Selective spectroscopy at low temperatures revealing spectral disorder effects of the LH2 antenna excitons and exciton polarons

Considerable heterogeneity of spectral characteristics of purified LH complexes has been noticed [25–29,40,45–47,57,62,64,69–75]. The disorder effects are best studied at low temperatures when exciting with spectrally narrow excitation light at the red edge of the lowest-energy absorption band. As follows selective spectroscopy data for purified and membrane LH2 complexes are compared and discussed. The previous selective spectroscopy studies [25,47,69,72] that primarily concerned isolated complexes agree with the present more detailed results.

Plotted in Fig. 5 as a function of excitation wavelength for isolated (black squares) and membrane (red dots) LH2 samples at 5 K are the fluorescence emission peak position (Fig. 5a), the energy gap between the excitation laser frequency and the fluorescence maximum frequency (Fig. 5b), and the FWHM of the emission spectrum (Fig. 5c). The energy gap and width parameters are defined in Fig. 6 below. Shown also in Fig. 5a with black and red drop lines are the respective inhomogeneously broadened distributions of the lowest-energy exciton polaron states (SDF) of the B850 aggregate in isolated and membrane LH2 complexes. The SDF is routinely measured as a distribution of the zero-phonon hole depths at constant burn fluence [25]. At low temperatures, the states from SDF are the origins of the fluorescence emission spectra. Both internal (intra-complex) and external (inter-complex) disorders contribute into the experimental SDF [40,73,76,77]. Random variations of diagonal (transition energies of the sites) and off-diagonal (exciton coupling) energies in each and every antenna complex cause the former disorder, while fluctuations of the mean transition energy of the Bchl sites in different B850 aggregates create the latter disorder. Only the internal disorder is subject to dynamic (motional) narrowing [78].

As can be seen from Fig. 5a, the SDF for the membrane samples is more red shifted and considerably broader than it is for isolated complexes. The SDF in isolated (membrane) complexes peaks at 864.9 ± 0.5 nm (870.0 ± 0.5 nm), its FWHM being 148 ± 10 cm^{-1} (202 ± 15 cm^{-1}). The numbers for isolated complexes match well the previously reported data from this [70] as well as other laboratories [27,29]. The redder position of the membrane SDF is rather expected from the above comparison of the absorption spectra. The somewhat larger peak shift of SDF (5.1 nm) than the absorption spectra (3.3 nm) is also understandable. According to the simplified disordered Frenkel exciton model [5,21,76], the B850 absorption peak is related to the $k = \pm 1$ exciton states, while the lowest state, to the $k = 0$ state (see

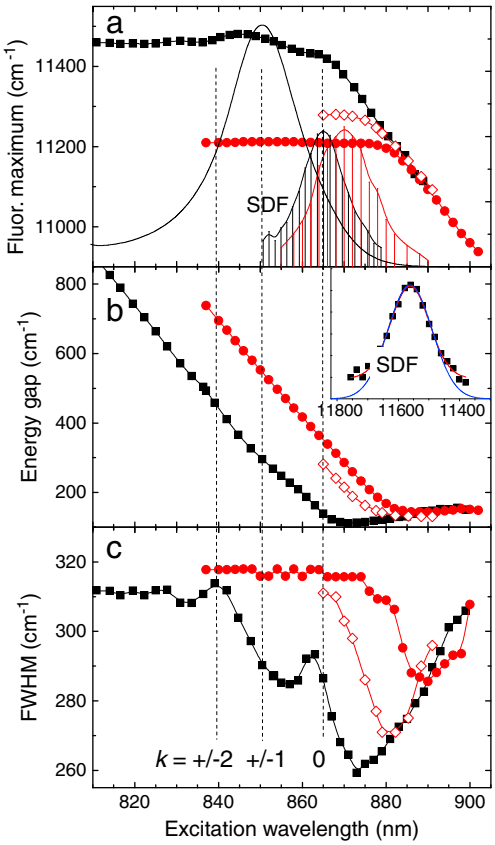

Fig. 5. The fluorescence peak position (a), energy gap (b), and FWHM (c) characteristics of selective spectra for isolated (black squares) and membrane (red dots) LH2 complexes measured at 5 K as a function of excitation wavelength. The SDF distributions in panel (a), arbitrarily scaled to the absorption spectrum of isolated complexes (black line, the same as in Figs. 2b and 4), are shown with black and red drop lines for isolated and membrane complexes, respectively. Solid lines connecting the scattered data points are for leading the eye. Vertical dashed lines indicate approximate mean peak positions of the exciton states in isolated complexes. The inset in panel (b) shows Gaussian fits of the experimental SDF (scattered). See text for further details.

the calculated density of the exciton states in Fig. 9b). The stronger exciton coupling in membranes evidenced by Fig. 4 results in larger energy gap between these states, pushing the lowest $k=0$ state further toward red. Furthermore, the excitation energy transfer between the inter-connected LH2 complexes in extended network of the membrane vesicles, in principle, tends to reduce hole-burning efficiency. The transfer processes, being more effective at higher energies, potentially suppress the blue side of the SDF, hence causing its apparent red shift. At the same time, both the latter mechanisms (increased exciton coupling and energy transfer) would be expected to bring in some narrowing of SDF. Considerably broader SDF in membranes thus speaks for increased internal and/or external disorders in the membrane environment, in conformity with the conventional absorption–fluorescence spectra in Fig. 2.

Different authors generally agree upon the peak positions of the SDF. However, the reported widths of SDF deviate considerably [25,27,29]. The FWHM obtained for isolated complexes varies between $135\pm10\ cm^{-1}$ [27] and $190\pm10\ cm^{-1}$ [29]. The present value of $148\pm10\ cm^{-1}$ agrees within the experimental uncertainty with the former number. The only previous estimate for the FWHM of SDF in membranes [25] is $60\ cm^{-1}$, in vast contrast with the present $202\pm15\ cm^{-1}$. It is usually not clarified how different authors deal with the so-called baseline problem. The inset of Fig. 5b illustrates the issue on the example of isolated complexes (see also [72]). To get FWHM of SDF discreet experimental points plotted in wavenumber scale are commonly fitted by a Gaussian function. Due to obvious experimental limitations, the wings of the measured distribution are poorly determined, leaving the fit somewhat ambiguous. The two possible limiting approximations in the inset are demonstrated with the red (zero baseline, FWHM equal to $148\pm10\ cm^{-1}$) and blue (with baseline, $170\pm10\ cm^{-1}$) curves. In the case of broader SDF in the membrane sample, however, the two estimates differ but a little: $202\pm15\ cm^{-1}$ versus $210\pm15\ cm^{-1}$.

The fluorescence maximum, energy gap, and FWHM dependences in Fig. 5 upon excitation with narrow laser line clearly demonstrate beginning of spectral selectivity at the long-wavelength tail of the absorption spectra close to the SDF maximum. The major selectivity features, all rather similar in both isolated and membrane LH2 samples include linearly correlated shift of the fluorescence spectrum with excitation wavelength (i) (Fig. 5a), and minimized energy gap (ii) (Fig. 5b) and emission bandwidth (iii) (Fig. 5c) values. The selectivity in membranes sets in at slightly longer wavelengths compared with isolated complexes, being associated with the redder position of their absorption and SDF bands. Remarkably, however, at the far-red edge of the absorption spectra past about 880 nm the peak, gap, and FWHM parameters for isolated and membrane samples practically coincide.

The various bumps and wiggles apparent in the curves of isolated complexes that roughly correlate with spectral positions of the higher-energy exciton states, first of all the ±1 states at around 850 nm and the ±2 states at around 840 nm (indicated in Fig. 5 with dashed lines), show that limited spectral selectivity is present even with respect to these states (see also [47,69]). Considerably larger inhomogeneous broadening and fast energy transfer specified below washes out these structures in the membranes. As seen in Fig. 5a, the fluorescence band position is rather insensitive to the excitation frequency in the high-energy range. This is the Kasha–Vavilov's rule at work in excitonically coupled system. The energy gap (Fig. 5b), which initially decreases almost linearly with excitation wavelength, goes through a minimum and starts to rise. The minimum gap value in isolated complexes, where selectivity is better, is $111\ cm^{-1}$. The behavior of the fluorescence bandwidth (Fig. 5c) is most complex. It reflects an intricate interplay of spectral selectivity and exciton polaron properties. Qualitatively, however, the FWHM dependence follows that for the energy gap. The long-wavelength rise of the gap and FWHM is related to the already noted increase of the homogeneous spectral width and electron–phonon coupling strength. As demonstrated in [72], all these features can be reasonably well reproduced theoretically.

Interesting dichotomy has been observed for the *Rb. sphaeroides* membrane data. There appears to be two regular types of samples whose fluorescence spectra at non-selective excitation are typically shifted relative to each other by 60–70 cm^{-1}. Representative characteristics of these samples are in Fig. 5 indicated by red filled rings and red open diamonds. Heterogeneous variants of *Rb. sphaeroides* membranes have been found (R. Cogdell, private communication). Alternative possibility is that the two sample sorts represent solutions of well-isolated membrane vesicles and their fused-together aggregates. This latter combination might then have redder spectrum.

3.4. Homogeneous exciton polaron lineshapes in dependence of the excitation wavelength

We have already noted that almost all specific differences between the isolated and membrane samples seem to vanish at long wavelengths above about 880 nm. This implies similar physical properties of the photo-excitations in these samples. Here, we provide the results of a detailed study of the homogenous line shapes of light-harvesting exciton polarons in isolated and membrane LH2 complexes obtained by ΔFLN spectroscopy [49]. Low fluences below ~1 J/cm^2 are applied to avoid spurious excitation intensity effects [72] (see Table 1).

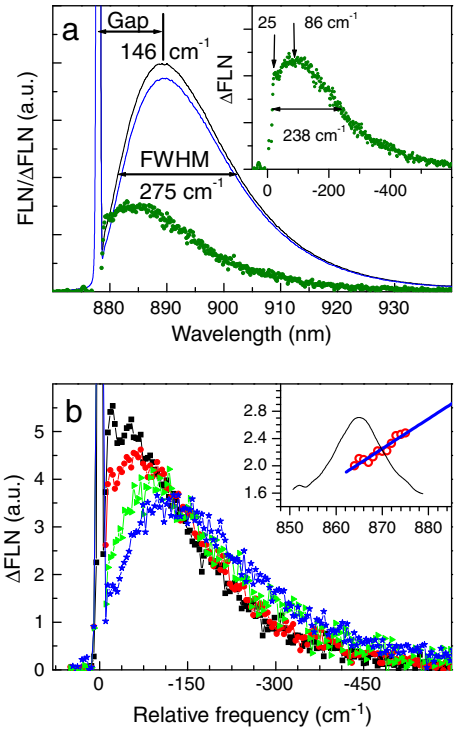

Fig. 6. ΔFLN spectra of membrane (a, olive scattered line) and isolated (b) LH2 complexes from *Rb. sphaeroides* at 4.5 K. Shown in part (a) with black and blue lines are the pre- and post-burn FLN spectra, respectively. The inset presents ΔFLN spectrum in frequency scale. The area-normalized spectra in part (b) are measured at following excitation wavelengths: 869 nm (black), 877 nm (red), 885 nm (green), and 889 nm (blue). The inset shows the Huang–Rhys factor, *S*, dependence on excitation wavelength on the background of the SDF (the same as in Fig. 5a). Blue line denotes linear fit of the experimental data (red dots).

Shown in Fig. 6a with olive scattered line is the ΔFLN (homogeneous) spectrum for the membrane LH2 complexes at 878-nm excitation. This wavelength corresponds to about half intensity of the respective SDF from the long-wavelength side (see Fig. 5). The same spectrum albeit in energy scale is drawn in the inset of Fig. 6a. To demonstrate clearly the phonon wing (PW) structure of the spectrum, the intense ZPL at spectral origin is removed. As can be seen, the phonon sideband of 238 cm^{-1} FWHM peaks at 86 cm^{-1}. There is as well a low-frequency structure at ~25 cm^{-1}. (The latter two frequencies are counted relative to the ZPL origin.) Fig. 6a also presents the pre-burn (black line) and post-burn (blue line) FLN spectra in order to show the energy gap and FWHM measures of the selective spectra used in Fig. 5. In these FLN spectra the ZPL are truncated at a few percent intensity levels. Fig. 6b provides the ΔFLN spectra for isolated complexes. The spectra normalized with respect to PW areas are measured at different wavelengths along the long-wavelength tail of the absorption spectrum. The increasing Stokes shift of the PW maximum, its broadening, and loss of fine structure

Table 1
The phonon sideband parameters of isolated LH2 complexes from *Rb. sphaeroides* as a function of the excitation wavelength.

Excitation wavelength (nm)	Absorbed energy density[a] (J/cm^2)	Gap[b] (cm^{-1})	FWHM (cm^{-1})	*S*[c]
869	0.07	48	164	2.2
877	0.17	61	194	2.5
885	0.06	89	231	2.9
889	0.11	111	259	3.1

[a] Estimated from the excitation intensity and OD of the sample.
[b] Estimated as the energy difference between the ZPL and PW peaks (see Fig. 6).
[c] Based on linear extrapolation of the data shown in the inset of Fig. 6.

present a clear evidences of growing exciton–phonon coupling strength with excitation wavelength, in very good agreement with our earlier studies [23,72].

The exciton–phonon coupling strength (also called the Huang–Rhys factor), *S*, can be evaluated from the experimental spectra as:

$$S(\lambda_{ex}) = \ln[1 + I_{PW}(\lambda_{ex})/I_{ZPL}(\lambda_{ex})], \quad (3)$$

where $I_{PW}(\lambda_{ex})$ and $I_{ZPL}(\lambda_{ex})$ are, respectively, the integral intensities of PW and ZPL at the particular excitation wavelength λ_{ex}. The *S* dependence on λ_{ex} for LH2 complexes at 4.5 K is demonstrated in the inset of Fig. 6b. Representative values of the gap, FWHM, and *S* parameters for the isolated LH2 complexes as a function of excitation wavelength are collected in Table 1.

The ΔFLN spectra of isolated and membrane LH2 complexes almost overlie at the red edge of the spectra, which of course is not surprising, given the data of Fig. 5 discussed earlier. It is also important to notice that very similar selective spectroscopy data as described in Sections 3.3 and 3.4 with respect to the LH2 complexes from *Rb. sphaeroides* have been obtained for LH2 and LH3 complexes from *Rps. acidophila* as well as for a mutant LH2 complex from *Rb. sphaeroides*, which lacks the B800 molecules. These facts imply generality of the obtained results.

3.5. Nanosecond excited state decay as a function of temperature and fluorescence emission wavelength

Fig. 7 depicts temperature dependences of the relative (with respect to the 5 K value) fluorescence yield, *Q*, and decay time, τ, for isolated and membrane LH2 complexes in the range of 5–300 K. While the yield measurements accounted for the whole emission spectrum, in the lifetime measurements the fluorescence was recorded at 870 nm (complexes) or at 890 nm (membranes) with 4-nm or 12-nm slit widths, respectively.

The yield and lifetime dependences are similar for separate samples but appear very different if the data sets for isolated complexes are compared with those for the membrane complexes. In isolated complexes, in agreement with previous reports [28,57], the *Q* and τ values stay constant at low temperatures up to ~175 K and then gradually decline by 30–35% at ambient temperature. In membranes, in contrast, the temperature-induced drop of these parameters begins immediately at the lowest temperature continuing all the way up to ambient temperatures, where only about 20% of their initial value is left. Such strong quenching of the membrane emission can be understood within the already used paradigm of structural and spectral heterogeneity of the energetically inter-connected network of LH2 complexes. Occasional quenchers (of still unidentified nature)

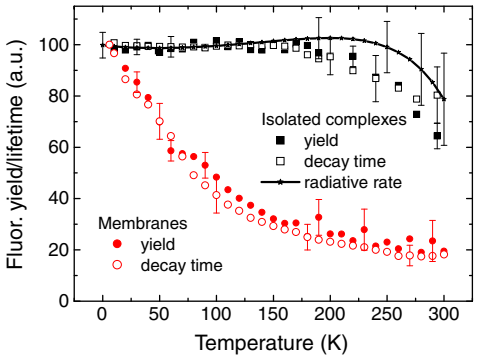

Fig. 7. Relative fluorescence yield (filled symbols) and decay time (open symbols) of isolated (black squares) and membranes (red rings) LH2 complexes from *Rb. sphaeroides* as a function of temperature. The solid black line represents the relative radiative decay rate for the isolated complexes.

localized in separate membrane areas become increasingly available for quenching with raising temperature.

The nearly parallel dependences of Q and τ found both in isolated and membrane samples imply constant radiative decay rate

$$r_{rad} = \frac{Q}{\tau}. \quad (4)$$

This is certainly true in case of isolated complexes at low temperatures, as shown by solid black line in Fig. 7. Yet the present data do not allow such strong conclusions toward physiological temperatures due to rising experimental uncertainty at high temperatures, especially in membranes.

Fig. 8a demonstrates significant fluorescence decay time dependence on recording wavelength in both isolated and membrane LH2 complexes at 5 K. The fluorescence was excited at 800 nm and recorded with spectral resolution of 4 nm. The longest lifetime in isolated complexes ($\tau = 1.73 \pm 0.02$ ns) is recorded at the blue edge (854 nm) of the emission spectrum. Toward longer wavelengths the τ gradually shortens, reaches a minimum value of ~1.1 ns at ~913 nm, and then rises again until around 950 nm it stabilizes at 1.29–1.30 ns level. The wavelength dependence of τ weakens with raising temperature, being completely wiped out at ambient temperatures [57,79]. Qualitatively very similar spectral and kinetic behaviors are observed in isolated LH2 and LH3 complexes from *Rps. acidophila* (see Table 2). Alas, although first reported for the LH2 complexes from *Rb. sphaeroides* already a decade ago [57,71], this strong lifetime dependence on the emission wavelength has been completely ignored in the scientific literature. The spectral dependences described above almost certainly reflect fundamental properties of the light-harvesting exciton polarons [23,58,72].

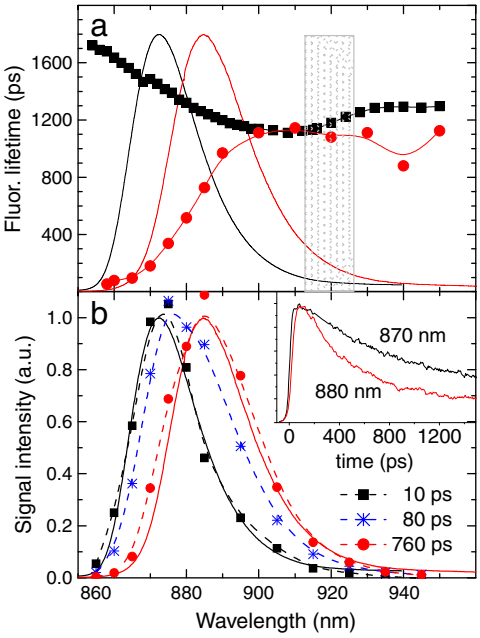

Fig. 8. (a) Fluorescence decay times at 5 K in isolated (black squares) and membrane (red rings, estimated according to Eq. (5)) LH2 complexes from *Rb. sphaeroides* as a function of recording wavelength. The peak-normalized reference steady-state fluorescence emission spectra are presented with respectively colored continuous lines. The gray area indicates onset of the lifetime increase for the isolated complexes. Solid lines connecting the scattered data points are for leading the eye. (b) Peak-normalized transient fluorescence emission spectra at different picosecond delay times (symbols and dashed lines) relative to steady-state fluorescence spectra of isolated and membrane samples (continuous lines, same as in part (a)). The spectra are constructed following Eq. (2). The inset shows examples of decay kinetics for isolated (black) and membrane (red) LH2 complexes, recorded at 870 nm and 880 nm, respectively.

Table 2
Variations of the fluorescence decay time (±0.02 ns) in isolated LH2 and LH3 complexes along the fluorescence spectrum at 5 K.

Sample	Decay time (ns)		
	Blue edge	Intermediate	Red edge
LH2 (*Rb. sphaeroides*)	1.73 (854 nm)	1.1 (913 nm)	1.30 (950 nm)
LH2 (*Rps. acidophila*)	1.74 (878 nm)	1.25 (928 nm)	
LH3 (*Rps. acidophila*)	2.04 (826 nm)	1.28 (890 nm)	1.51 (926 nm)

As for the surprising increase of the emission lifetime around 915–930 nm in Fig. 8a, it might be related to the decay of the blue-edge exciton polarons in the B850 aggregates with simultaneous creation of high-frequency local vibrations of the constituting Bchl molecules in the ground state. The line of logic goes as follows. According to [35,80], the Q_y transition in Bchl molecules is strongest coupled to the group of modes around 726 and 900 cm^{-1}. Downshifting the blue edge of the fluorescence spectrum, where the longest τ have been measured, by 726–900 wavenumbers yields 912–926 nm, almost precisely the region of the lifetime growth. Vibronic structure of the emission spectrum expected in this range (highlighted in Fig. 7b with a gray-hatched quarter) is too weak to be distinguishable under nonselective excitation; however, it can be recorded with selective excitation (paper under preparation).

In membranes not only the spectral dependence but also the fluorescence decay kinetics are significantly different from those in isolated complexes. While in isolated complexes the nearly mono-exponential decay is observed at all temperatures, in membranes the kinetics is generally non-exponential (see the inset of Fig. 8b), enforcing the use of average (weighted) lifetimes as follows:

$$\tau = \frac{\sum_i A_i \tau_i}{\sum_i A_i}. \quad (5)$$

As can be seen from Fig. 8b, the low-temperature behavior of such-calculated average membrane emission lifetimes is quite opposite to that for isolated complexes. The lifetime is short (in the range of 30 ps) at the blue edge of the emission spectrum and increases gradually toward longer wavelengths. The longest lifetime, close to the shortest lifetime in isolated complexes, is reached past 900 nm.

Dispersive kinetics have earlier been observed in the membranes of purple bacteria that only develop core antenna complexes [62,81], and explained [52,62–65,82,83] by use of directed excitation energy transfer in the spectrally inhomogeneous antenna system from high-energy complexes to the lower-energy ones. The funneling of the excitation energy into the lowest-energy states is expected to result in time-dependent spectral red shift. Such shift in tens to hundreds of picosecond time range can be easily followed at low temperatures in the membrane LH2 samples, as shown in Fig. 8b. The transient spectra in this time window roughly shift between the steady-state spectral positions of isolated and membrane samples. The transient spectrum at 760-ps delay is somewhat broader than the steady-state membrane spectrum. This implies long transfer times for considerable number of relaxation routes, the times that are comparable to the nanosecond excited state lifetime.

3.6. Exciton state-selective femtosecond transient absorption spectra

According to the present wisdom, the electronic excitations in the B850 ring upon a short, femtosecond-pulse excitation are excitons that are partially localized by static spectral disorder [32,33,84]. The dynamic (temperature-induced) disorder that sets in with a time delay causes a structural relaxation of the lattice and further stabilization of the exciton in the form of an exciton polaron [23,57,69]. This exciton polaron relaxation is known to occur in the LH2

bacterial antennas with a time constant on the order of 10^{-13} s [26,39,45,46,85,86].

As follows we are comparing the transient pump-probe differential absorption spectra of isolated and membrane LH2 complexes upon spectrally narrow (5 nm FWHM) pulse excitation. The narrow pump pulses are applied to resonantly excite selected exciton states under the apparently smooth absorption bandshape. The used approximately Gaussian pump pulse shapes with respect to the absorption spectrum of the isolated LH2 complexes at 5 K are shows in Fig. 9a. Demonstrated in Fig. 9b are the calculated low-temperature absorption spectrum of an ensemble of the spectrally disordered B850 aggregates of LH2 (red line) and the corresponding distribution of the exciton states (DOS, black bold line). The shapes drawn with thin black line represent ensemble distributions of the 18 individual exciton states: $k=0, -1, +1, -2,\ldots +8, 9$, as counted from the low-energy side. The model parameters and simulation details can be found in [23]. The excitation pulses have possibly been chosen to spectrally overlap with the main peaks of DOS, as shown in Fig. 9b.

Fig. 10 presents the transient absorption difference spectra of isolated and membrane LH2 complexes recorded at various delay times between the 200-fs pump and probe pulses. The time zero is arbitrarily defined as the time when the signal first time surpasses the noise level. The spectra chosen for the presentation are excited (from top to bottom) at blue side (840 nm), at maximum (850 nm), and at the very red edge of the B850 absorption band (874 nm in complexes and 880 nm in membranes). As can be checked from Fig. 9, these excitations roughly overlap with the $k=\pm2$, $k=\pm1$, and $k=0$ exciton states, respectively. The same states appeared prominent with respect to selective spectroscopy data (see Fig. 5). The transient difference spectra generally consist from positive- and negative-sign parts that correspondingly represent radiation absorption from the optically excited electronic state (further termed as the excited-state absorption, ESA), and a combined effect of bleaching of the ground state absorption (GSA) and stimulated emission from the excited electronic state (SE).

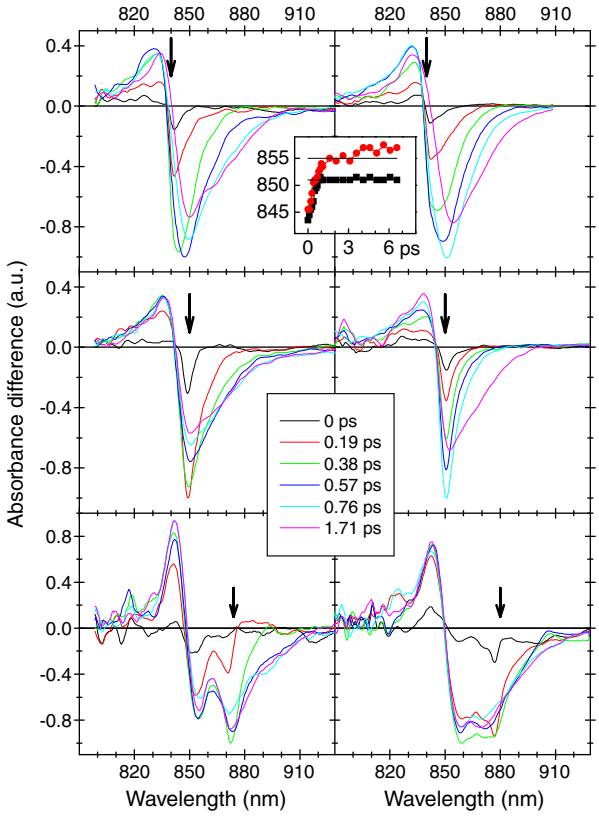

Fig. 10. Transient differential absorption spectra of isolated (left column) and membrane (right column) LH2 complexes at 10 K recorded at various indicated pump wavelengths (arrows) and delay times between the 200 fs pump and probe pulses. The inset shows the bleaching maximum position at the 840-nm excitation for isolated (black squares) and membrane (red dots) LH2 complexes as a function of delay time, adapted from [39]. Solid lines connecting the scattered data points are for leading the eye.

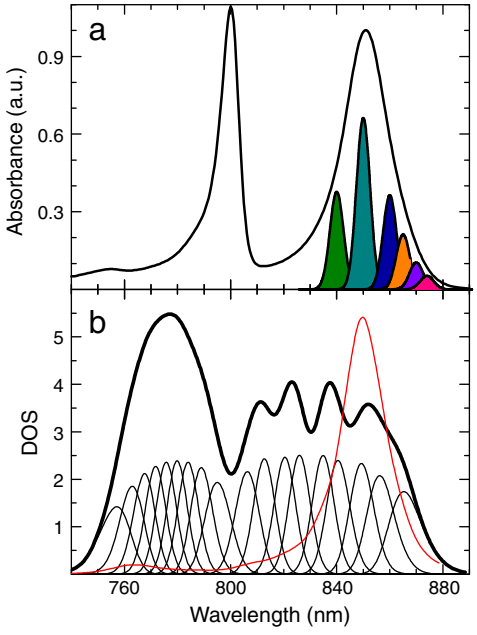

Fig. 9. (a) The 5 nm broad excitation pulse shapes (filled areas) and the absorption spectrum of the isolated LH2 complexes at 5 K (the same as in Figs. 2 and 4). (b) The calculated low-temperature absorption spectrum of an ensemble of the spectrally disordered B850 aggregates of LH2 (red line) and the corresponding distribution of the exciton states (DOS, black bold line), adapted from [23]. The thin black line shapes represent ensemble distributions of individual exciton states. See text for further details.

From the very first sight it is clear that the spectra of the complexes in Fig. 10 are more clear-cut than those of the membranes. This is consistent with the above conclusion of larger spectral disorder in membranes. As one might expect, the initial, femtosecond time-range spectral dynamics significantly depends on excitation wavelength. While at high-energy excitations of 840/850 nm, it takes time for the bleached part of the spectrum to relax into a two-peak structure, the same structure is there from the outset in case of the low-energy excitation of 874/880 nm. At the latter excitation, both samples acquire clear, stable two-peak structure, which still is more structured in isolated complexes. These two spectral peaks, one at ~850 nm and the second, at 870–880 nm originate from the GSA and SE, respectively (see Fig. 11 for more detailed discussion).

Essentially different dynamics of transient spectra in case of isolated and membrane LH2 complexes is evident from the inset of Fig. 10, where the position of the bleaching maximum is plotted against the pump-probe delay time. The initially similar dynamics, which involve the spectral shape evolution and red shift by almost 10 nm clearly diverge for the two samples past about 1 ps. While in isolated complexes the shift ceases, in membranes it continues into hundreds of picoseconds to nanosecond time range. This slow dynamics has been attributed to energy transfer processes among the spectrally inhomogeneous antennas of the extended photosynthetic membrane [39,45,46]. Origin of the initial fast dynamics plainly seen in isolated LH2 complexes is quite different. It is due to the exciton polaron relaxation [39]. Another estimate of this characteristic can be obtained from SE rise time measurements. Recorded between 860 and 910 nm, the SE rise time varies between 100 and 300 fs (not shown), in good agreement with the previous estimate [39].

Note worthily, the relaxed spectra measured at a "long", a few picosecond delay times depend on excitation wavelength not only in isolated but also in membrane samples (Fig. 11). The spectra shift progressively to the red at longer excitation wavelengths. Moreover, the spectra excited at longer wavelengths develop more clear-cut structure. This is similar to the behavior we met above in the selective spectroscopy part and can naturally be explained analogously: by selective excitation within inhomogeneously broadened absorption spectra in the corresponding samples. At the far-red excitation, 874/880 nm, the bleach signal has two clearly distinguishable dips. The higher-energy dip is related to the GSA, while that at lower energy, to SE of an excited sub-population of the LH2 complexes. The splitting between the two dips, nearly the same at various pump wavelengths, is comparable with the Stokes shift of the low-temperature absorption and emission spectra in Fig. 2.

4. Summary

In the present work, spectroscopic and kinetic fingerprints have been established that characterize the lowest-energy B850 electronic transitions in individual detergent-solubilized and membrane-embedded LH2 antenna complexes from the photosynthetic purple bacterium *Rb. sphaeroides*. A few comparative data are also provided for LH2 and LH3 complexes from *Rps. acidophila*. Significant changes in energetics and dynamics of the antenna excitons upon self-assembly of the proteins into intracytoplasmic membranes have been observed and interpreted. The main conclusions drawn from these studies are as follows.

(i) Slight but characteristic differences between the shapes of functionally most relevant lowest-energy absorption/fluorescence spectra of the LDAO-solubilized and the native membrane-embedded LH2 complexes of *Rb. sphaeroides* exist over the whole 4–300 K temperature range.

(ii) The membrane spectra are generally redder and broader than the respective spectra of isolated complexes. The relative shift of the absorption spectra is a prime result of a reduced exciton coupling in isolated LH2, most probably because of a loosened package of the protein scaffold in detergent micelles. Excitation energy transfer between the LH2 complexes present in membranes and absent in isolated complexes dominates the fluorescence spectral variations in these samples.

(iii) Bigger inhomogeneous broadening in membranes explains their broader spectra at low temperatures. At the same time, the homogenous spectral characteristics of the B850 photoexcitations revealed under selective excitation in isolated and membrane LH2 complexes are rather similar. They imply strong exciton–phonon coupling ($S \geq 2$) and, consequently, the existence of exciton polarons/self-trapped excitons in the thermally equilibrated light-harvesting complexes.

(iv) Relaxation of the initially excited excitons into exciton polarons/self-trapped excitons in the B850 antenna aggregates takes at low temperatures a few hundred femtoseconds. The complex excitation energy transfer present only in membranes proceeds on an extended time scale from picosecond to a nanosecond.

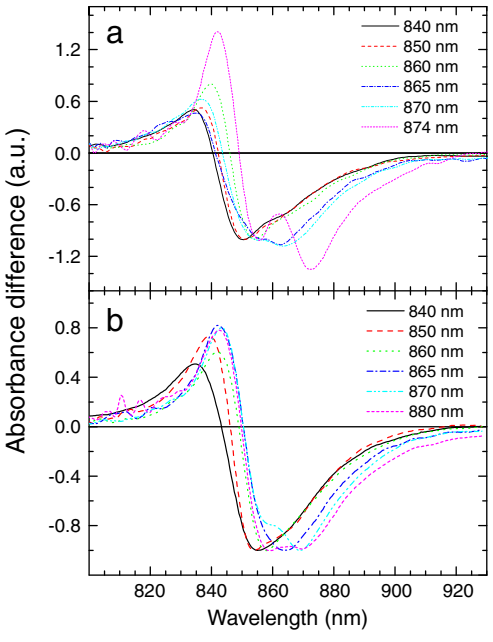

Fig. 11. Difference absorption spectra in isolated (a) and membrane (b) LH2 complexes at different indicated excitation wavelengths. The spectra are recorded at a "long" delay time 1.8 ps.

Many authors (see, e.g., [87] and references therein) have reported about reversible shifts of the room-temperature absorption spectra of bacterial antenna proteins upon variation of the detergent concentration. In our own experience, we have learned that decreasing the LDAO concentration down the level where the LH2 complexes start to stick together (the critical concentration being ≤100 detergent molecules per LH2 protein [22]) leads to a gradual red shift of the absorption/emission spectra, a none single-exponential fluorescence decay, and other effects typical for the aggregates that support excitation energy transfer between its monomeric subunits. All the observed spectral and kinetic modifications take place between the limits set by isolated complexes from one side and intact membranes from another side. These results thus indicate robust and practical spectral and kinetic criteria for discrimination against aggregation of the photosynthetic light-harvesting complexes. We hope that the present data also contribute into understanding of various elements related to stabilization, purification, and storage of the membrane proteins.

Acknowledgements

Estonian Science Foundation (Grant No. 8674) and Ministry of Education and Science (Grant SF0180055s07) supported this work. J.-A. Williams and N.W. Woodbury generously donated the *Rb. sphaeroides* strains with the puf operon, and T. Gillbro the LH2 and LH3 complexes from *Rps. acidophila*. D. Dolak (*Protein-Solutions Inc.*) kindly provided the data presented in Fig. 1; M. Pajusalu participated in the experiments resulting in Fig. 4. The femtosecond transient spectroscopy measurements were carried out during the leave of K.T and A.F. at Arizona State University. The authors are grateful to N.W. Woodbury for hospitality and S. Lin for expert support with instrumentation.

References

[1] A. Schubert, A. Stenstam, W.J.D. Beenken, J.L. Herek, R.J. Cogdell, T. Pullerits, S. V., In vitro self-assembly of the light harvesting pigment–protein LH2 revealed by ultrafast spectroscopy and electron microscopy, Biophys. J. 86 (2004) 2363–2373.
[2] R.E. Blankenship, Molecular Mechanisms of Photosynthesis, Blackwell Science, Oxford, 2002.
[3] M.R. Jones, G.J.S. Fowler, L.C.D. Gibson, G.G. Grief, J.D. Olsen, W. Crielaard, C.N. Hunter, Mutants of *Rhodobacter sphaeroides* lacking one or more pigment–protein complexes and complementation with reaction-center, LH1, and LH2 genes, Mol. Microbiol. 6 (1992) 1173–1184.
[4] A.Y. Borisov, A.M. Freiberg, V.I. Godik, K. Rebane, K. Timpmann, Kinetics of picosecond bacteriochlorophyll luminescence in vivo as a function of the reaction center state, Biochim. Biophys. Acta 807 (1985) 221–229.
[5] H. Van Amerongen, L. Valkunas, R. Van Grondelle, Photosynthetic Excitons, World Scientific, Singapore, 2000.
[6] R.N. Frese, C.A. Siebert, R.A. Niederman, C.N. Hunter, C. Otto, R. van Grondelle, The long-range organization of a native photosynthetic membrane, Proc. Natl. Acad. Sci. U. S. A. 101 (2004) 17994–17999.

[7] M. De Rivoyre, N. Ginet, P. Bouyer, J. Lavergne, Excitation transfer connectivity in different purple bacteria: a theoretical and experimental study, Biochem. Biophys. Acta 1797 (2010) 1780–1794.
[8] S. Bahatyrova, R.N. Frese, C.A. Siebert, J.D. Olsen, K.O. van der Werf, R. van Grondelle, R.A. Niederman, P.A. Bullough, C. Otto, C.N. Hunter, The native architecture of a photosynthetic membrane, Nature 430 (2004) 1058–1062.
[9] S. Scheuring, D. Levy, J.-L. Rigaud, Watching the components of photosynthetic bacterial membranes and their in situ organization by atomic force microscopy, Biochem. Biophys. Acta 1712 (2005) 109–127.
[10] S. Scheuring, J.N. Sturgis, Atomic force microscopy of the bacterial photosynthetic apparatus: plain pictures of an elaborate machinery, Photosynth. Res. 102 (2009) 197–211.
[11] J.N. Sturgis, R.A. Niederman, Atomic force microscopy reveals multiple patterns of antenna organization in purple bacteria: implications for energy transduction mechanisms and membrane modeling, Photosynth. Res. 95 (2008) 269–278.
[12] J.N. Sturgis, J.D. Tucker, J.D. Olsen, C.N. Hunter, R.A. Niederman, Atomic force microscopy studies of native photosynthetic membranes, Biochemistry 48 (2009) 3679–3698.
[13] J.D. Tucker, C.A. Siebert, M. Escalante, P. Adams, J.D. Olsen, C. Otto, D.L. Stokes, C.N. Hunter, Membrane invagination in *Rhodobacter sphaeroides* is initiated at curved regions of the cytoplasmic membrane, then forms both budded and fully detached spherical vesicles, Mol. Microbiol. 76 (2010) 833–847.
[14] G. McDermott, S.M. Prince, A.A. Freer, A.M. Hawthornthwaite-Lawless, M.Z. Papiz, R.J. Cogdell, N.W. Isaacs, Crystal structure of an integral membrane light-harvesting complex from photosynthetic bacteria, Nature 374 (1995) 517–521.
[15] T. Walz, S.J. Jamieson, C.M. Bowers, P.A. Bullough, C.N. Hunter, Projection structures of three photosynthetic complexes from *Rhodobacter sphaeroides*: LH2 at 6 A, LH1 and RC-LH1 at 25 A, J. Mol. Biol. 282 (1998) 833–845.
[16] J.D. Olsen, J.D. Tucker, J.A. Timney, P. Qian, C. Vassilev, C.N. Hunter, The organization of LH2 complexes in membranes from *Rhodobacter sphaeroides*, J. Biol. Chem. 283 (2008) 30772–30779.
[17] G.J.S. Fowler, G.D. Sockalingum, B. Robert, C.N. Hunter, Blue shifts in bacteriochlorophyll absorbance correlate with changed hydrogen bonding patterns in light-harvesting 2 mutants of *Rhodobacter sphaeroides* with alterations at.alpha.-Tyr-44 and.alpha.-Tyr-45, Biochem. J. 299 (1994) 695–700.
[18] A. Gall, G.J.S. Fowler, C.N. Hunter, B. Robert, Influence of the protein binding site on the absorption properties of the monomeric bacteriochlorophyll in *Rhodobacter sphaeroides* LH2 complex, Biochemistry 36 (1997) 16282–16287.
[19] J.N. Sturgis, J.D. Olsen, B. Robert, C.N. Hunter, Functions of conserved tryptophan residues of the core light-harvesting complex of *Rhodobacter sphaeroides*, Biochemistry 36 (1997) 2772–2778.
[20] V. Sundström, T. Pullerits, R. van Grondelle, Photosynthetic light-harvesting: reconciling dynamics and structure of purple bacterial LH2 reveals function of photosynthetic unit, J. Phys. Chem. B 103 (1999) 2327–2346.
[21] R.J. Cogdell, A. Gall, J. Köhler, The architecture and function of the light-harvesting apparatus of purple bacteria: from single molecules to in vivo membranes, Q. Rev. Biophys. 39 (2006) 227–324.
[22] L. Kangur, K. Timpmann, A. Freiberg, Stability of integral membrane proteins against high hydrostatic pressure: the LH2 and LH3 antenna pigment–protein complexes from photosynthetic bacteria, J. Phys. Chem. B 112 (2008) 7948–7955.
[23] A. Freiberg, G. Trinkunas, Unraveling the hidden nature of antenna excitations, in: A. Laisk, L. Nedbal, Govindjee (Eds.), Photosynthesis in Silico, Understanding Complexity From Molecules to Ecosystems, Springer, Heidelberg, 2009, pp. 55–82.
[24] A. Freiberg, K. Timpmann, G. Trinkunas, Spectral fine-tuning in excitonically coupled cyclic photosynthetic antennas, Chem. Phys. Lett. 500 (2010) 111–115.
[25] N.R.S. Reddy, R. Picorel, G.J. Small, B896 and B870 components of the *Rhodobacter sphaeroides* antenna: a hole burning study, J. Phys. Chem. 96 (1992) 6458–6464.
[26] R. Jimenez, S.N. Dikshit, S.E. Bradforth, G.R. Fleming, Electronic excitation transfer in the LH2 complex of *Rhodobacter sphaeroides*, J. Phys. Chem. 100 (1996) 6825–6834.
[27] H.-M. Wu, M. Rätsep, R. Jankowiak, R.J. Cogdell, G.J. Small, Comparison of the LH2 antenna complexes of *Rhodopseudomonas acidophila* (strain 10050) and *Rhodobacter sphaeroides* by high-pressure absorption, high-pressure hole burning, and temperature-dependent absorption spectroscopies, J. Phys. Chem. B 101 (1997) 7641–7653.
[28] R. Monshouwer, M. Abrahamsson, F. van Mourik, R. van Grondelle, Superradiance and exciton delocalization in bacterial photosynthetic light-harvesting systems, J. Phys. Chem. B 101 (1997) 7241–7248.
[29] R. Purchase, S. Völker, Spectral hole burning: examples from photosynthesis, Photosynth. Res. 101 (2009) 245–266.
[30] O. Zerlauskiene, G. Trinkunas, A. Gall, B. Robert, V. Urboniene, L. Valkunas, Static and dynamic protein impact on electronic properties of light-harvesting complex LH2, J. Phys. Chem. B 112 (2008) 15883–15892.
[31] V. Urboniene, O. Vrublevskaja, G. Trinkunas, A. Gall, B. Robert, L. Valkunas, Solvation effect of bacteriochlorophyll excitons in light-harvesting complex LH2, Biophys. J. 93 (2007) 2188–2198.
[32] D. Leupold, H. Stiel, K. Teuchner, F. Nowak, W. Sandner, B. Uecker, H. Scheer, Size enhancement of transition dipoles to one- and two-exciton bands in a photosynthetic antenna, Phys. Rev. Lett. 77 (1996) 4675–4678.
[33] L.D. Book, A.E. Ostafin, N. Ponomarenko, J.R. Norris, N.F. Scherer, Exciton delocalization and initial dephasing dynamics of purple bacterial LH2, J. Phys. Chem. B 104 (2000) 8295–8307.
[34] S. Georgakopoulous, R.N. Frese, E. Johnson, C. Koolhaas, R.J. Cogdell, R. Van Grondelle, G. Van der Zwan, Absorption and CD spectroscopy and modeling of various LH2 complexes from purple bacteria, Biophys. J. 82 (2002) 2184–2197.
[35] M. Rätsep, Z.-L. Cai, J.R. Reimers, A. Freiberg, Demonstration and interpretation of significant asymmetry in the low-resolution and high-resolution Qy fluorescence and absorption spectra of bacteriochlorophyll a, J. Chem. Phys. 134 (2011) 024506.
[36] H. Lesch, J. Schlichter, J. Friedrich, J.M. Vanderkooi, Molecular probes: what is the range of their interaction with the environment? Biophys. J. 86 (2004) 467–472.
[37] C.N. Hunter, H.J.M. Kramer, R. Van Grondelle, Linear dichroism and fluorescence emission of antenna complexes during photosynthetic unit assembly in *Rhodopseudomonas sphaeroides*, Biochim. Biophys. Acta 807 (1985) 44–51.
[38] R.J. Van Dorssen, C.N. Hunter, R. Van Grondelle, A.H. Korenhof, J. Amesz, Spectroscopic properties of antenna complexes of *Rhodobacter sphaeroides* in vivo, Biochim. Biophys. Acta 932 (1988) 179–188.
[39] K. Timpmann, N.W. Woodbury, A. Freiberg, Unraveling exciton relaxation and energy transfer in LH2 photosynthetic antennas, J. Phys. Chem. B 104 (2000) 9769–9771.
[40] R. Agarwal, A.H. Rizvi, B.S. Prall, J.D. Olsen, C.N. Hunter, G.R. Fleming, Nature of disorder and inter-complex energy transfer in LH2 at room temperature: a three pulse photon echo peak shift study, J. Phys. Chem. A 106 (2002) 7573–7578.
[41] L. Kangur, K. Leiger, A. Freiberg, Evidence for high-pressure-induced rupture of hydrogen bonds in LH2 photosynthetic antenna pigment–protein complexes, J. Phys. Conf. Ser. 121 (2008) 112004.
[42] T.J. Pflock, S. Oellerich, L. Krapf, J. Southall, R.J. Cogdell, G.M. Ullmann, J. Köhler, The electronically excited states of LH2 complexes from *Rhodopseudomonas acidophila* and dynamic Monte Carlo simulations. I. Isolated, non-interacting LH2 complexes, J. Phys. Chem. B 115 (2011) 8821–8831.
[43] T.J. Pflock, S. Oellerich, J. Southall, R.J. Cogdell, G.M. Ullmann, J. Köhler, The electronically excited states of LH2 complexes from *Rhodopseudomonas acidophila* and dynamic Monte Carlo simulations. I. Isolated, non-interacting LH2 complexes, J. Phys. Chem. B 115 (2011) 8813–8820.
[44] D.J. Dawkins, L.A. Ferguson, R. Cogdell, The structure of the 'core' of the purple bacterial photosynthetic unit, in: H. Scheer, S. Schneider (Eds.), Photosynthetic Light-Harvesting Systems: Organization and Function, Walter de Gruyter and Co., Berlin and New York, 1988, pp. 115–127.
[45] A. Freiberg, J.A. Jackson, S. Lin, N.W. Woodbury, Subpicosecond pump-supercontinuum probe spectroscopy of LH2 photosynthetic antenna proteins at low temperature, J. Phys. Chem. A 102 (1998) 4372–4380.
[46] A. Freiberg, K. Timpmann, S. Lin, N.W. Woodbury, Exciton relaxation and transfer in the LH2 antenna network of photosynthetic bacteria, J. Phys. Chem. B 102 (1998) 10974–10982.
[47] A. Freiberg, M. Rätsep, K. Timpmann, G. Trinkunas, Self-trapped excitons in circular bacteriochlorophyll antenna complexes, J. Lumin. 102–103 (2003) 363–368.
[48] O. Sild, K. Haller (Eds.), Zero-Phonon Lines and Spectral Hole Burning in Spectroscopy and Photochemistry, Springer Verlag, Berlin, Heidelberg, 1988.
[49] M. Rätsep, A. Freiberg, Resonant emission from the B870 exciton state and electron–phonon coupling in the LH2 antenna chromoprotein, Chem. Phys. Lett. 377 (2003) 371–376.
[50] A. Freiberg, P. Saari, Picosecond spectrochronography, IEEE J. Quantum Electron. QE-19 (1983) 622–630.
[51] A. Freiberg, Primary processes of photosynthesis studied by fluorescence spectroscopy methods, Laser Chem. 6 (1986) 233–252.
[52] A. Freiberg, V.I. Godik, T. Pullerits, K. Timpman, Picosecond dynamics of directed excitation transfer in spectrally heterogeneous light-harvesting antenna of purple bacteria, Biochim. Biophys. Acta 973 (1989) 93–104.
[53] L. Valkunas, V. Liuolia, A. Freiberg, Picosecond processes in chromatophores at various excitation intensities, Photosynth. Res. 27 (1991) 83–95.
[54] A. Freiberg, S. Lin, K. Timpmann, R.E. Blankenship, Exciton dynamics in FMO bacteriochlorophyll protein at low temperatures, J. Phys. Chem. B 101 (1997) 7211–7220.
[55] W. Brown (Ed.), Dynamic Light Scattering, the Method and Some Applications, Oxford University Press, Oxford, U.K., 1993
[56] X. Hong, Y.-X. Weng, M. Li, Determination of the topological shape of integral membrane protein light-harvesting complex LH2 from photosynthetic bacteria in the detergent solution by small-angle X-ray scattering, Biophys. J. 86 (2004) 1082–1088.
[57] A. Freiberg, M. Rätsep, K. Timpmann, G. Trinkunas, N.W. Woodbury, Self-trapped excitons in LH2 antenna complexes between 5 K and ambient temperature, J. Phys. Chem. B 107 (2003) 11510–11519.
[58] M. Pajusalu, M. Rätsep, G. Trinkunas, A. Freiberg, Davydov splitting of excitons in cyclic bacteriochlorophyll a nanoaggregates of bacterial light-harvesting complexes between 4.5 and 263 K, ChemPhysChem 12 (2011) 634–644.
[59] C.P. Rijgersberg, R. Van Grondelle, J. Amesz, Energy transfer and bacteriochlorophyll fluorescence in purple bacteria at low temperature, Biochim. Biophys. Acta 592 (1980) 53–64.
[60] K. Timpmann, G. Trinkunas, J.D. Olsen, C.N. Hunter, A. Freiberg, Bandwidth of excitons in LH2 bacterial antenna chromoproteins, Chem. Phys. Lett. 398 (2004) 384–388.
[61] K. Timpmann, G. Trinkunas, P. Qian, C.N. Hunter, A. Freiberg, Excitons in core LH1 antenna complexes of photosynthetic bacteria: evidence for strong resonant coupling and off-diagonal disorder, Chem. Phys. Lett. 414 (2005) 359–363.
[62] A. Freiberg, V.I. Godik, T. Pullerits, K.E. Timpmann, Directed picosecond excitation transport in purple photosynthetic bacteria, Chem. Phys. 128 (1988) 227–235.
[63] C.N. Hunter, H. Bergstroem, R. Van Grondelle, V. Sundstroem, Energy-transfer dynamics in three light-harvesting mutants of *Rhodobacter sphaeroides*: a picosecond spectroscopy study, Biochemistry 29 (1990) 3203–3207.
[64] K. Timpmann, A. Freiberg, V.I. Godik, Picosecond kinetics of light excitations in photosynthetic purple bacteria in the temperature range of 300–4 K, Chem. Phys. Lett. 182 (1991) 617–622.

[65] T. Pullerits, K.J. Visscher, S. Hees, V. Sundstroem, A. Freiberg, K. Timpmann, R. van Grondelle, Energy transfer in the inhomogeneously broadened core antenna of purple bacteria: a simultaneous fit of low-intensity picosecond absorption and fluorescence kinetics, Biophys. J. 66 (1994) 236–248.
[66] S. Scheuring, AFM studies of the supramolecular assembly of bacterial photosynthetic core-complexes, Curr. Opin. Chem. Biol. 10 (2006) 387–393.
[67] S. Scheuring, T. Boudier, J.N. Sturgis, From high-resolution AFM topographs to atomic models of supramolecular assemblies, J. Struct. Biol. 159 (2007) 268–276.
[68] K.K. Rebane, Impurity Spectra of Solids, Plenum Press, New York, 1970.
[69] K. Timpmann, Z. Katiliene, N.W. Woodbury, A. Freiberg, Exciton self-trapping in one-dimensional photosynthetic antennas, J. Phys. Chem. B 105 (2001) 12223–12225.
[70] K. Timpmann, M. Rätsep, C.N. Hunter, A. Freiberg, Emitting excitonic polaron states in core LH1 and peripheral LH2 bacterial light-harvesting complexes, J. Phys. Chem. B 108 (2004) 10581–10588.
[71] A. Freiberg, M. Rätsep, K. Timpmann, G. Trinkunas, Dual fluorescence of single LH2 antenna nanorings, J. Lumin. 108 (2004) 107–110.
[72] A. Freiberg, M. Rätsep, K. Timpmann, G. Trinkunas, Excitonic polarons in quasi-one-dimensional LH1 and LH2 bacteriochlorophyll a antenna aggregates from photosynthetic bacteria: a wavelength-dependent selective spectroscopy study, Chem. Phys. 357 (2009) 102–112.
[73] A.M. Van Oijen, M. Ketelaars, J. Köhler, T.J. Aartsma, J. Schmidt, Spectroscopy of individual light-harvesting complexes of *Rhodopseudomonas acidophila*: diagonal disorder, intercomplex heterogeneity, spectral diffusion, and energy transfer in the B800 band, Biophys. J. 78 (2000) 1570–1577.
[74] R. Jankowiak, M. Reppert, V. Zazubovich, J. Pieper, T. Reinot, Site selective and single complex laser-based spectroscopies: a window on excited state electronic structure, excitation energy transfer, and electron–phonon coupling of selected photosynthetic complexes, Chem. Rev. 111 (2011) 4546–4598.
[75] M. Rätsep, C.N. Hunter, J.D. Olsen, A. Freiberg, Band structure and local dynamics of excitons in bacterial light-harvesting complexes revealed by spectrally selective spectroscopy, Photosynth. Res. 86 (2005) 37–48.
[76] A. Freiberg, K. Timpmann, R. Ruus, N.W. Woodbury, Disordered exciton analysis of linear and nonlinear absorption spectra of antenna bacteriochlorophyll aggregates: LH2-only mutant chromatophores of *Rhodobacter sphaeroides* at 8 K under spectrally selective excitation, J. Phys. Chem. B 103 (1999) 10032–10041.
[77] M. Ketelaars, A.M. van Oijen, M. Matsushita, J. Köhler, J. Schmidt, T.J. Aartsma, Spectroscopy on the B850 band of individual light-harvesting 2 complexes of *Rhodopseudomonas acidophila* I. Experiments and Monte Carlo simulations, Biophys. J. 80 (2001) 1591–1603.
[78] Y. Toyozawa, Optical Processes in Solids, Cambridge University Press, Cambridge, 2003.
[79] T. Pflock, M. Dezi, G. Venturoli, R.J. Cogdell, J. Köhler, S. Ollerich, Comparison of the fluorescence kinetics of detergent-solubilised and membrane-reconstituted LH2 complexes from *Rps. acidophila* and *Rb. sphaeroides*, Photosynth. Res. 95 (2008) 291–298.
[80] M. Rätsep, A. Freiberg, Electron–phonon and vibronic couplings in the FMO bacteriochlorophyll a antenna complex studied by difference fluorescence line narrowing, J. Lumin. 127 (2007) 251–259.
[81] A. Freiberg, V.I. Godik, K. Timpmann, Spectral dependence of the fluorescence lifetime of *Rhodospirillum rubrum*. Evidence for inhomogeneity of B880 absorption band, in: J. Biggins (Ed.), Progress in Photosynthesis Research, Nijhoff, Dordrecht, The Netherlands, 1987, pp. 45–48.
[82] T. Pullerits, A. Freiberg, Picosecond fluorescence of simple photosynthetic membranes: evidence of spectral inhomogeneity and directed energy transfer, Chem. Phys. 149 (1991) 409–418.
[83] T. Pullerits, A. Freiberg, Kinetic model of primary energy transfer and trapping in photosynthetic membranes, Biophys. J. 63 (1992) 879–896.
[84] O. Kuhn, V. Sundstrom, Pump-probe spectroscopy of dissipative energy transfer dynamics in photosynthetic antenna complexes: a density matrix approach, J. Chem. Phys. 107 (1997) 4154–4164.
[85] Y.-Z. Ma, R.J. Cogdell, T. Gillbro, Energy transfer and exciton annihilation in the B800-850 antenna complex of the photosynthetic purple bacterium *Rhodopseudomonas acidophila* (Strain 10050). A femtosecond transient absorption study, J. Phys. Chem. B 101 (1997) 1087–1095.
[86] J.T.M. Kennis, A.M. Streltsov, S.I.E. Vulto, T.J. Aartsma, T. Nozawa, J. Amesz, Femtosecond dynamics in isolated LH2 complexes of various species of purple bacteria, J. Phys. Chem. B 101 (1997) 7827–7834.
[87] P.A. Loach, P.S. Parkes-Loach, Structure–function relationships in bacterial light-harvesting complexes investigated by reconstitution techniques, in: C.N. Hunter, F. Daldal, M.C. Thurnauer, J.T. Beatty (Eds.), The Purple Photosynthetic Bacteria, Springer, Dordrecht, 2008, pp. 181–198.